New alternative of design and control of grid connected PV-Storage systems with the five level diode clamped inverter

Kamal. Himour[1], Kaci. Ghedamsi[1] and El Madjid. Berkouk[2]

1. *Laboratory of Renewable Energy Mastery, University of bejaia, 06000 Bejaia, Algeria.*
e-mail: himour.kamal@ Hotmail.fr,kghedamsi@yahoo.fr
2. *Laboratory of control process, ENP, Algiers, Algeria.*
e-mail: emberkouk@yahoo.fr

Abstract—**This paper aimed to evaluate the use of photovoltaic-battery storage systems to supply electric power in the distribution grid through a multilevel inverter. The proposed system is composed by four PV generators with MPPT (P&O) control, four battery storage systems connected to each capacitor of the DC link and a five level diode clamped inverter connected to the grid by a traditional three phase transformer. The proposed control has a hierarchical structure with both a grid side control level to regulate the power and the current injected to the grid and four input side regulation units. The system operators controls the power production of the four PV generators by sending out reference power signals to each input side regulation unit, the input side regulation units regulates the voltage of each capacitor of the DC link, regulates the voltage and the state of charge of the battery storage system connected to each PV generator.**

Keywords- **Photovoltaic generator, MPPT, Battery bank, five level diode clamped inverter, space vector modulation, supervision.**

I. INTRODUCTION

With the increasing concern about global environmental protection, the need to produce pollution-free natural energy such as solar energy has received great interest as an alternative source of energy for the future since solar energy is clean, pollution-free and inexhaustible. In an effort to use the solar energy effectively, a great deal of research has been done on the grid connected photovoltaic generation systems [1-4]. In PV systems connected to the grid, the inverter that converts the output direct voltage of the solar modules to the alternate voltage (AC) is receiving increased interest in order to generate power to utility.

In order to inject power on demand, certain energy storage devices must be added into the system. These devices must Store PV energy in excess of electricity demand and subsequently meet electricity demand in excess of PV energy. The conventional lead–acid battery is the most common energy storage device at the present time [5].

Another very important aspect of the systems connected to the grid is to select a proper power factor according to the grid demands: active or reactive power. The most efficient systems are those, which allow variation in the active and reactive power injected into the grid, depending on the power grid requirements [6]. In this scenario, we propose a control strategy for a photovoltaic- battery storage system connected to the grid with a five level diode clamped inverter.

So, this paper is organized as follows: in section 2 we presented the global model of the system: mathematical model of the photovoltaic generator, model of battery bank, model and control of the five level diode clamped inverter, Energy management and control structure. Then, in section 3 we presented the simulation results and we terminated by a conclusion of this study in section 4.

II. SYSTEM MODELLING

Fig. 1 shows the configuration of the grid-connected PV battery storage system, which consists of four PV generators , four DC/DC converters for MPPT, four battery bank connected to the DC link by four bidirectional DC-DC converter and the five level diode clamped inverter connected to the grid through a traditional three phase transformer.

ISSN: 2356-5608

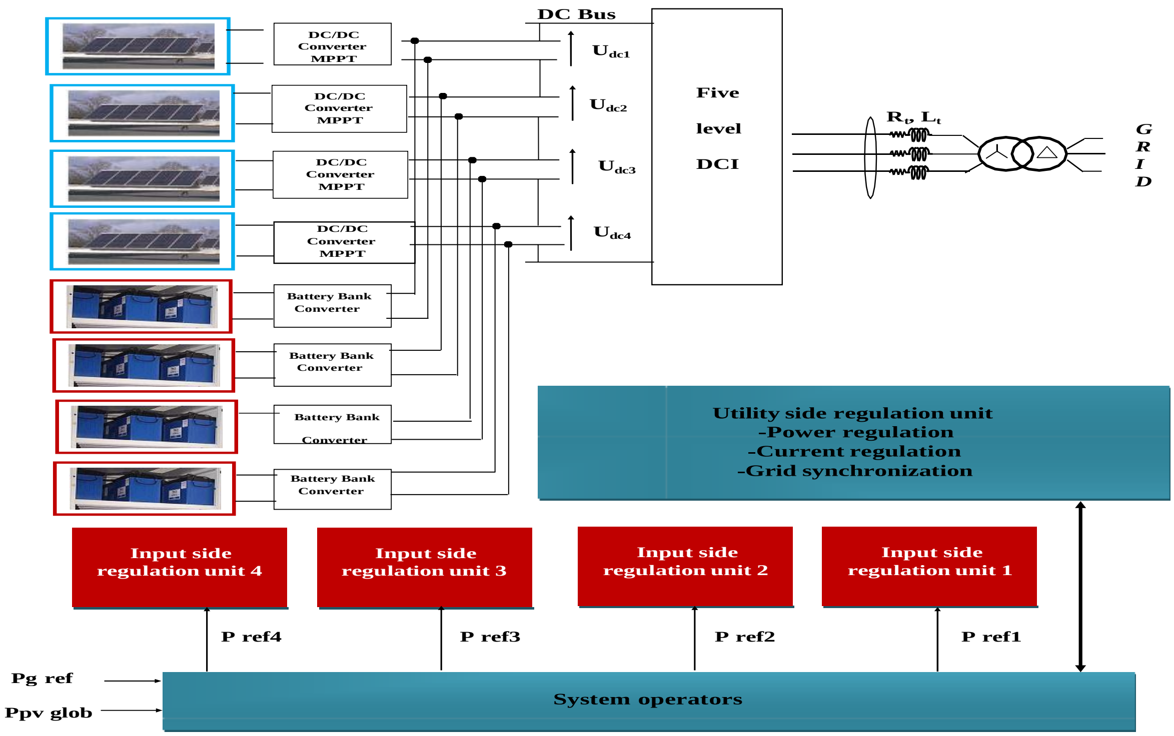

Fig. 1. The basic structure of the three phase grid connected PV-Battery storage system.

The control structure of the proposed system is composed of two structures control:

1. The grid side control unit which the main property is:
- control the active power injected into the grid,
- control and regulate the reactive power;
- ensure high quality of the injected power;
- Grid synchronization.

2. Four input side regulation units which have the goal to:
- regulate the voltage of each capacitor of the DC link ,
- regulate the voltage and the state of charge of storage systems.

A. Model of PV generator

The PV generator consists of electrically connected PV modules and it is modeled by physical oriented equivalent circuits, including one or more diode. The single diode equivalent circuit as shown in Fig. 2 is the most commonly used model for large PV generators [7].

The mathematical model witch relates the output current to the output voltage is given by the following expression:

$$I = I_{ph} - I_s\left[\left(\exp\frac{V + I.R_s}{m.\frac{K.T}{q}}\right) - 1\right] - \frac{V + I.R_s}{R_{sh}} \quad (1)$$

Where:

I_{ph}: The photo-current, I_s: the saturation current of diode, m: ideality factor, R_s and R_{sh} : series and parallel resistance, T: junction temperature, K: Boltzmann constant, q : electron charge.

For a PV module with N_s series connected cells and N_p parallel connected cells, the current-voltage characteristic is given by:

$$I = N_p.I_{ph} - N_p.I_s\left[\exp\left(\left(\frac{1}{m.K.\frac{T}{q}}\right).\left(\frac{V}{N_s} + \frac{R_s.I}{N_p}\right)\right) - 1\right] - \frac{N_p}{R_{sh}}.\left(\frac{V}{N_s} + \frac{R_s.I}{N_p}\right) \quad (2)$$

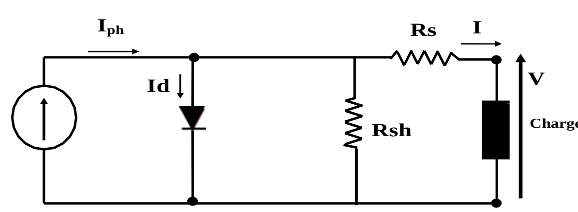

Fig. 2. Photovoltaic cell equivalent circuit.

B. Maximum power point tracking

The PV array must operate electrically at a certain voltage which corresponds to the maximum power point under the given operating conditions. To do this, a maximum power point tracking (MPPT) technique should be applied.

ISSN: 2356-5608

Various MPPT techniques like look-up table methods, perturbation and observation (P & O) methods and computational methods have been proposed in the literature. The perturb and observe(P&O), as the name itself states that the algorithm is based on the observation of the array output power and on the perturbation (increment or decrement) of the power based on increments of the array voltage or current. The algorithm continuously increments or decrements the reference current or voltage based on the value of the previous power sample. The P&O is the simplest method which senses the PV array voltage and the cost of implementation is less and hence easy to implement

C. Battery bank model

Lead acid batteries are used to guarantee several hours to a few days of energy storage. The model representation of the lead-acid battery is shown in Fig. 3. The capacity of the battery is determined by integrating the main reaction current I_{MR} . To consider the increased gassing losses when charging the battery at high voltage and temperature, here represented by the loss-current I_{gas}, constitutes a significant improvement over alternative battery models for the simulation of hybrid energy systems. The state-of-charge can be calculated by referring the actual capacity to the rated capacity of the battery, as expressed by equation 2 [8-9].

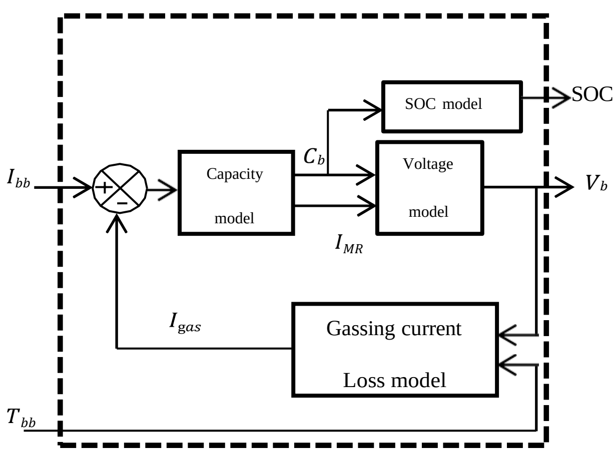

Fig.3. General structure of battery model.

The main reaction current of the battery bank can be expressed as:

$$I_{MR}(t) = I_{bb}(t) - I_{gas}(t) \quad (3)$$

Where:
I_{MR} : Main battery reaction current (A)
I_{bb}: External battery current (A)
I_{gas}: Battery gassing current (A)

The capacity model of the battery does not limit the charge or discharge current. Operation of the system with excessive charge or discharge currents has to be prevented by the selection of appropriately sized components and the implementation of a suitable control strategy. The actual battery capacity can be determined as:

$$C_b(t) = \int_{t=0}^{t} I_{MR}(t)\,dt + C_{b,i} \quad (4)$$

Where:
C_b: Actual battery capacity (Ah)
$C_{b,i}$: Initial battery capacity (Ah)

The state-of-charge can be calculated by referring the actual capacity to the rated capacity of the battery:

$$SOC(t) = \frac{C_b(t)}{C_{10}} \times 100\ \% \quad (5)$$

The presented voltage model of the battery is based on the 'Expanded Kinetic Battery Model', which has been presented in [14].
The voltage model considers that the battery terminal voltage depends on the following factors:
- Battery state-of-charge;
- Internal battery resistance;
- Magnitude and direction of battery current

For all calculations shown, different model parameters represent the characteristic voltage behaviour of lead-acid batteries when charging or discharging. The internal battery voltage is calculated as:

a) Charging ($I_{bb} < 0$)

$$E_b(t) = E_{0,c} + A_c.X(t) + \frac{C_c.X(t)}{(D_c - X(t))^{EFC}} \quad (6)$$

b) Discharging ($I_{bb} > 0$)

$$E_b(t) = E_{0,d} + A_D.X(t) + \frac{C_d X(t)}{(D_d - X(t))^{EFd}} \quad (7)$$

Where:
E_b: Internal battery voltage (V)
X: Normalised maximum charge/discharge capacity (Ah)

The normalised maximum charge/discharge capacity X is given as:

a) Charging ($I_{bb} < 0$)

$$X(t) = \frac{Q_{max,c}}{Q_{max}.(I_{MR}(t))} C_b(t) \quad (8)$$

b) Discharging ($I_{bb} > 0$)

$$X(t) = \frac{Q_{max,d}(Q_{max,d} - C_b(t))}{Q_{max}(I_{MR}(t))} \quad (9)$$

ISSN: 2356-5608

The maximum capacity Q_{max} in dependence of the main reaction current of the battery is expressed by a third order polynomial equation, where the parameters have to be determined by empirical curve fitting from measured data [14]:

a) Charging ($I_{bb} < 0$)

$$Q_{max}\left(I_{MR}(t)\right) = C_1.I_{MR}(t)^3 + C_2 I_{MR}(t)^2 + C_3 I_{MR}(t) + C_4 \qquad (10)$$

b) Discharging ($I_{bb} > 0$)

$$Q_{max}\left(I_{MR}(t)\right) = D_1.I_{MR}(t)^3 + D_2 I_{MR}(t)^2 + D_3 I_{MR}(t) + D_4 \qquad (11)$$

Therefore, the battery terminal voltage V_b can be calculated as:

a) Charging ($I_{bb} < 0$)

$$V_b(t) = E_b(t) - R_{0,c} I_{MR}(t) \qquad (12)$$

b) Discharging ($I_{bb} > 0$)

$$V_b(t) = E_b(t) - R_{0,d} I_{MR}(t) \qquad (13)$$

The voltage of a string of batteries is given by multiplying the battery voltage with the number of 12 Volt batteries in series:

$$V_{bb}(t) = B_s.V_b(t) \qquad (14)$$

where:
V_{bb} : Voltage of battery bank (V)
B_s: Number of 12 V batteries in series.

D. Model and control of the five level DCI

Multilevel converter gives massive advantages compared with conventional and very well-known two level converters like; high power quality waveforms, low switching losses, high voltage capability, low electromagnetic compatibility (EMC) etc. At the present time, the majority of research and development effort seems to concentrate on the development of three classes of inverters: the diode-clamped multilevel inverter, the multilevel inverter with cascaded single-phase H-bridge inverters and the multilevel inverter known as the flying capacitor inverter or some-times as the imbricate cells multilevel inverter [10-12].

1) Model of the five level DCI

A three-phase five-level diode-clamped inverter is shown in Fig.4 [13].

For each switch T_{ij} , we define the commutation function F_{ij} :

$$F_{ij} = \begin{cases} 1 & \text{if } S_{ij} \text{ is closed} \\ 0 & \text{otherwise} \end{cases} \qquad (15)$$

As indicated in table I, each leg of the inverter can have five possible switching states P_2, P_1 , O, N_1, N_2

TABLE I
STATES OF ONE LEG OF THE FIVE LEVEL DCI

Etat	S_{x1}	S_{x2}	S_{x3}	S_{x4}	S_{x5}	S_{x6}	S_{x7}	S_{x8}	V_{xo}
P_2	1	1	1	1	0	0	0	0	$U_c/2$
P_1	0	1	1	1	1	0	0	0	Uc/4
O	0	0	1	1	1	1	0	0	0
N_1	0	0	0	1	1	1	1	0	$-U_c/4$
N_2	0	0	0	0	1	1	1	1	$-U_c/2$

According to the states of the inverter, the output voltage vector can take several positions in the d-q frame. These positions are indicated on the space vector diagram Fig 5.

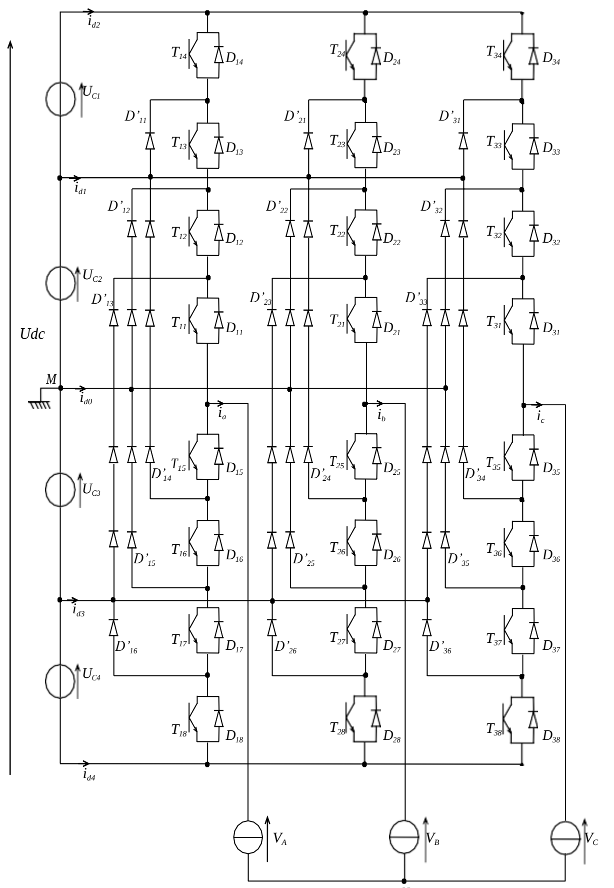

Fig.4. Five-level diode clamped inverter.

2) Simplified space vector modulation

In this paper, a new method is proposed in which the space vector diagram of five-level inverter is decomposed into six space vector diagrams of three level inverters. In turn, each of

ISSN: 2356-5608

these space vector diagrams of three level inverters is decomposed into six space vectors diagrams of two level inverters like showed in Fig 6. This modification can reduce considerably the computational time and reduce the algorithm complexity [14].

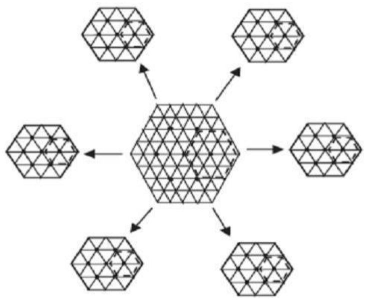

Fig.6. Decomposition of five level space vector diagram.

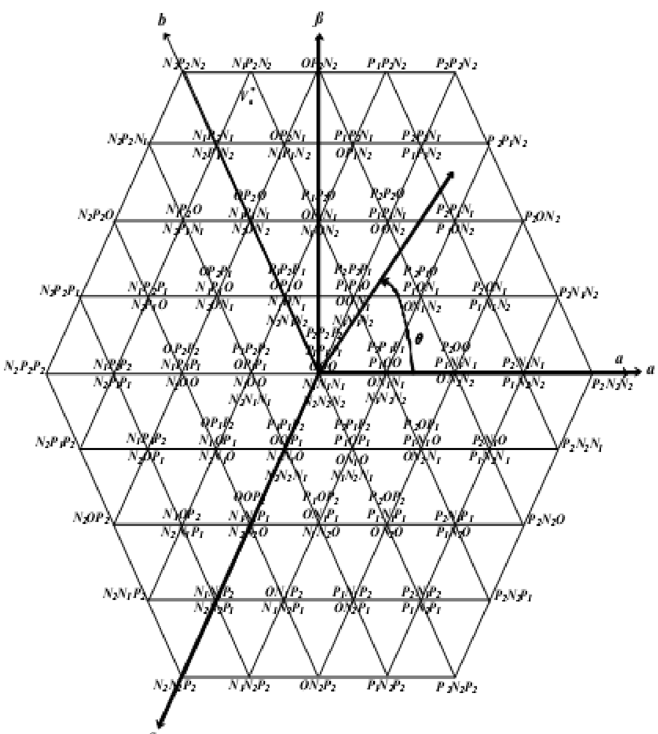

Fig.5. Space vector diagram of five-level inverter.

2.1. First correction of reference voltage vector

Having the location of a given reference voltage vector, one hexagon is selected among the six small hexagons that contain the five levels space vector diagram. Each hexagon is identified by a number s defined as given by:

$$s = \begin{cases} 1 \text{ if } \frac{-\pi}{3} \le \theta \le \frac{\pi}{3} \\ 2 \text{ if } \frac{\pi}{3} \le \theta \le \frac{\pi}{2} \\ 3 \text{ if } \frac{\pi}{2} \le \theta \le \frac{5.\pi}{6} \\ 4 \text{ if } \frac{5.\pi}{6} \le \theta \le \frac{7.\pi}{6} \\ 5 \text{ if } \frac{7.\pi}{6} \le \theta \le \frac{3.\pi}{2} \\ 6 \text{ if } \frac{3.\pi}{2} \le \theta \le \frac{11.\pi}{6} \end{cases} \quad (16)$$

After selection of one hexagon, we make a translation of the reference vector V_s^* towards the center of this hexagon.

TABLE II
FIRST CORRECTION OF REFERENCE VOLTAGE VECTOR

Hexagone	$V_d^{*'}$	$V_q^{*'}$
1	$V_d^* - 1/2$	V_q^*
2	$V_d^* - 1/4$	$V_q^* - \sqrt{3}/4$
3	$V_d^* + 1/4$	$V_q^* - \sqrt{3}/4$
4	$V_d^* + 1/2$	V_q^*
5	$V_d^* + 1/4$	$V_q^* + \sqrt{3}/4$
6	$V_d^* - 1/4$	$V_q^* + \sqrt{3}/4$

2.2. Second correction of reference voltage vector:

Having the selected three level inverter and the location of the translated vector, one hexagon is selected among the six small hexagons that contain this three level diagram. We make a translation of the reference $V_s^{*''}$. Table gives the components d and q of the reference voltage $V_s^{*''}$

TABLE III
SECOND CORRECTION OF REFERENCE VOLTAGE VECTOR

Hexagon	Component $V_d^{*''}$	Component $V_q^{*''}$
1	$V_d^{*'} - 1/4$	$V_q^{*'}$
2	$V_d^{*'} - 1/8$	$V_q^{*'} - \sqrt{3}/8$
3	$V_d^{*'} + 1/8$	$V_q^{*'} - \sqrt{3}/8$
4	$V_d^{*'} + 1/4$	$V_q^{*'}$
5	$V_d^{*'} + 1/8$	$V_q^{*'} + \sqrt{3}/8$
6	$V_d^{*'} - 1/8$	$V_q^{*'} + \sqrt{3}/8$

2.3. Determination of dwelling times

Ones the corrected reference voltage $V_s^{*''}$ and the corresponding hexagon are determined; we can apply the

ISSN: 2356-5608

conventional two level space vector Modulation method to calculate the dwelling times,

$$\begin{cases} T_1 = 4 * \left[\dfrac{\left|\overline{V_s^{*''}}\right|.T_s.\sin(\frac{\pi}{3}-\alpha)}{\sin(\frac{\pi}{3})}\right] \\ T_2 = 4 * \left[\dfrac{\left|\overline{V_s^{*''}}\right|.T_s.\sin(\alpha)}{\sin\left(\frac{\pi}{3}\right)}\right] \\ T_3 = T_s - T_1 - T_2 \end{cases} \qquad (17)$$

2.4. Conversion and sequence of the switching states

The reference voltage vector $V_s^{*''}$ is approximated using the nearest three states which are nodes of the triangle containing the vector identified as X, Y and Z. the optimum sequence of these states is selected so as to minimize the total number of switching transitions [13].

E. Energy management and control structure

The system operator controls the power production of the four PV generators by sending out reference power signals to each input side regulation unit.in this paper simply dispatching function distributes power reference to inside regulation units based on a Proportional distribution of the available active power.

$$P_{ref\ i} = \frac{P_{pv\ i}}{P_{pv\ global}}.P_{g\ ref} \qquad (18)$$

The control structure is composed of two main blocs:

1) Grid side regulation

Fig shows the structure of the grid side regulation [14-15].

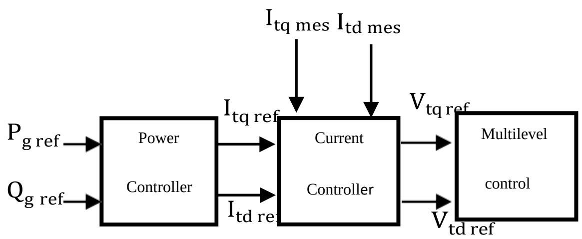

Fig.7. Bloc diagram grid side control.

1.1. Power control

The active and reactive power (P_g, Q_g) can be both expressed by using Park components of supply voltage (V_{td}, V_{tq}) and line current (I_{td}, I_{tq}) as follows:

$$\begin{cases} P_g = V_{td}.I_{td} + V_{tq}.I_{tq} \\ Q_g = V_{td}.I_{tq} - V_{tq}.I_{td} \end{cases} \qquad (19)$$

Reference currents ($I_{td\ ref}$, $I_{tq\ ref}$) which allows setting the desired reference active and reactive powers ($P_{g\ ref}$, $Q_{g\ ref}$), as follows:

$$\begin{cases} I_{td\ ref} = \dfrac{P_{g\ ref}.\hat{V}_{td} - Q_{g\ ref}.\hat{V}_{tq}}{\hat{V}_{td}^{\ 2} + \hat{V}_{tq}^{\ 2}} \\ I_{tq\ ref} = \dfrac{P_{g\ ref}.\hat{V}_{tq} + Q_{g\ ref}.\hat{V}_{td}}{\hat{V}_{td}^{\ 2} + \hat{V}_{tq}^{\ 2}} \end{cases} \qquad (20)$$

The unity power factor is obtained simply by setting the reactive power reference null. We can also generate or absorb ($Q_{g\ ref} < 0\ or\ Q_{g\ ref} > 0$).

1.2. Current control

The vector current control in Park reference frame is carried out by using the synchronized reference with the grid voltage. The electric equations of the filter (R_t, L_t) connected to the grid are given bellow:

$$\begin{cases} V_{td} = R_t I_{td} + L_t \dfrac{dI_{td}}{dt} - \omega_s L_t I_{td} + V_{gd} \\ V_{tq} = R_t I_{tq} + L_t \dfrac{dI_{tq}}{dt} + \omega_s L_t I_{tq} + V_{gq} \end{cases} \qquad (21)$$

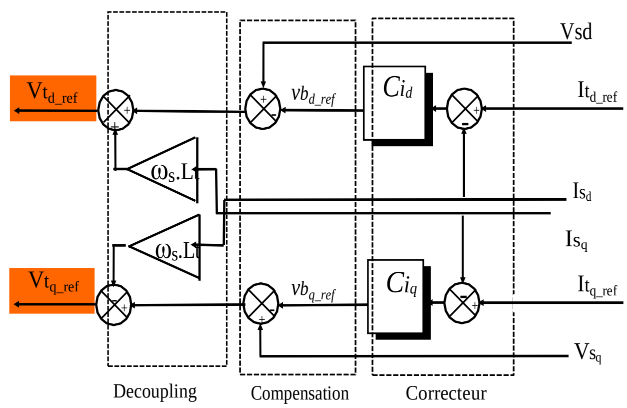

Fig.8. Bloc diagram of the current control.

1.3. Multilevel control

The five level diode clamped inverter is controlled by the simplified space vector modulation like presented in paragraph D.2.

2. Input side regulation units

The input side regulation units have two main objectives: regulation of battery bank storage system and regulation of the DC link capacitor with a PI corrector who gives the reference current to inject into the DC link capacitor.

ISSN: 2356-5608

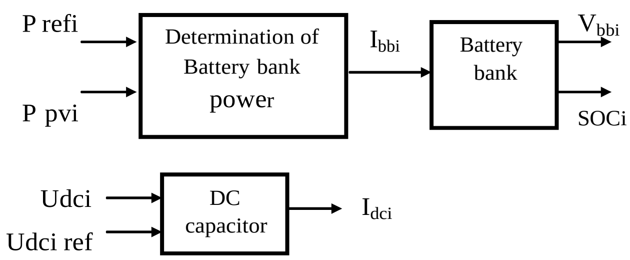

Fig.9. Input side control unit structure.

III. SIMULATION RESULTS

In this section, the photovoltaic grid connexion system is simulated using SIMULINK-MATLAB. PV generators have different irradiance profiles and each one is composed of five series modules connected to a DC-DC converter controlled by P&O strategy to track their maximum power point.

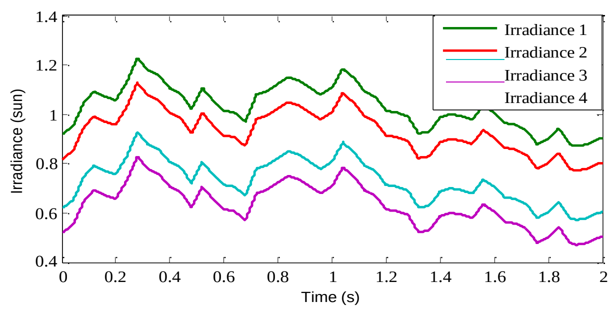

Fig.10. Profile irradiance of each PV generator.

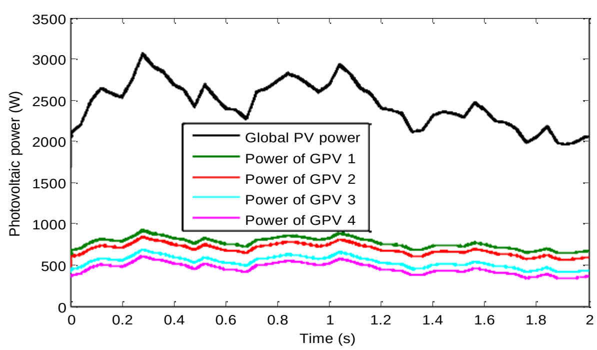

Fig.11. PV generators power (W).

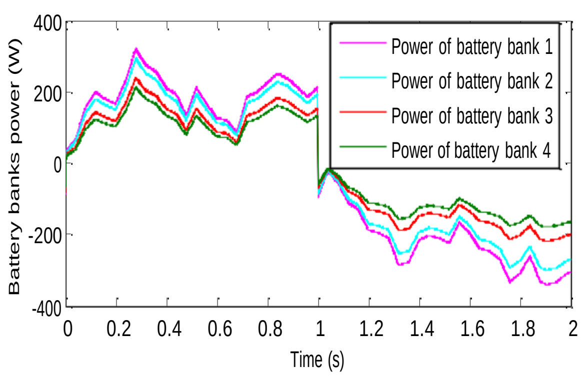

Fig.12. Battery banks power (W).

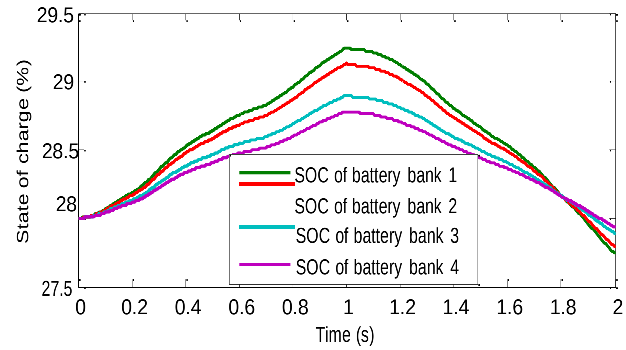

Fig.13. State of charge of battery banks.

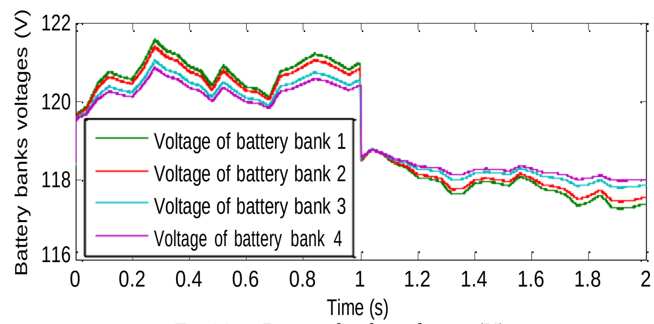

Fig.14. Battery banks voltages (V).

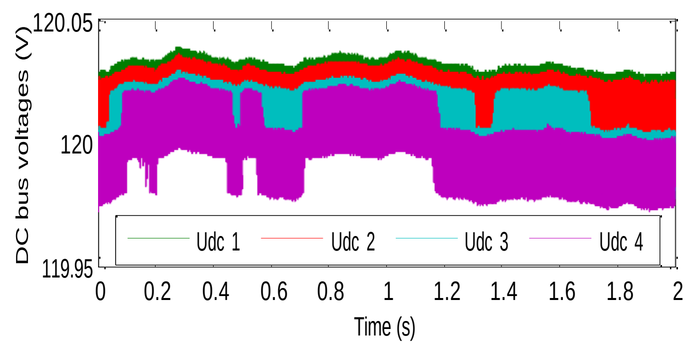

Fig.15. DC link capacitors voltages (V).

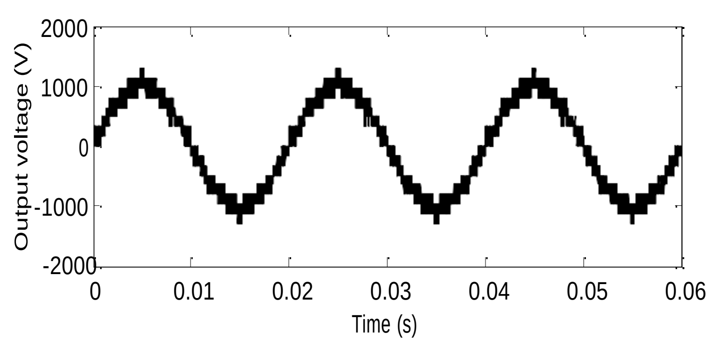

Fig.16. Phase 1 output voltage of 5 level inverter (V).

ISSN: 2356-5608

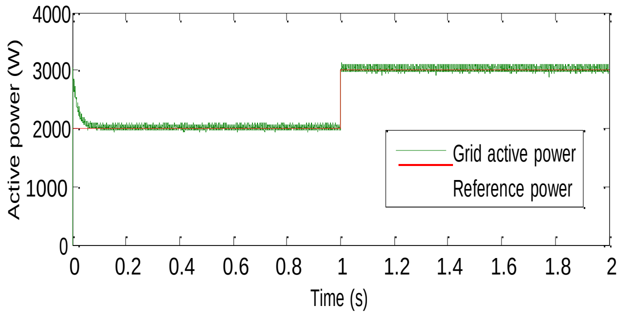

Fig.17. Grid active power (W).

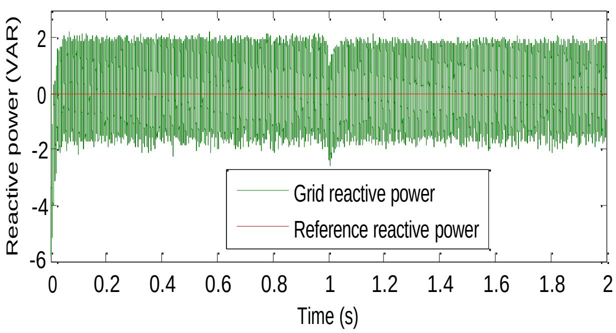

Fig.18. Grid reactive power (var)

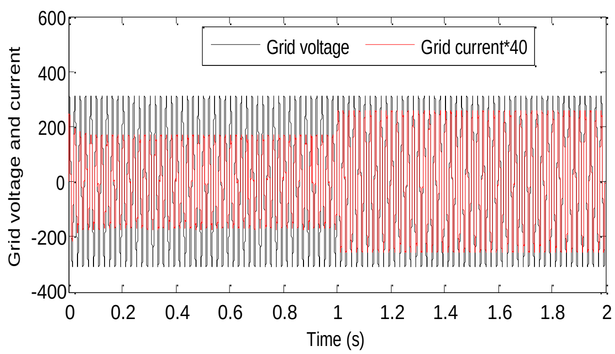

Fig.19. Grid currant (A) and grid voltage (V)

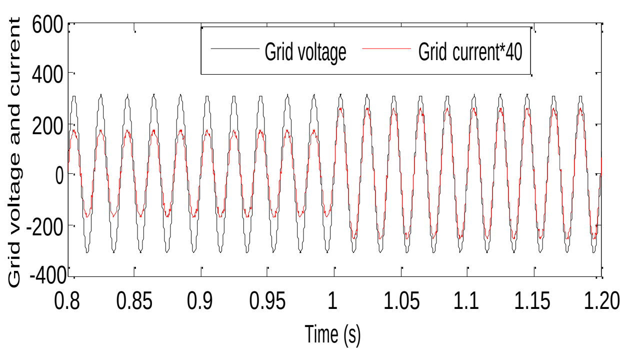

Fig.20. Zoom of grid currant (A) and grid voltage (V)

These simulation results improve the validity of the proposed control strategy for the grid PV/battery storage system. The results show that it is possible to inject to the grid a fixed power whatever solar irradiance and temperature condition as shouwn in Fig.17 and 18. The DC link voltage is maintined constant (Fig 15) , the multivel inverter gives a good quality energy (Fig. 16) . in Fig.19 and 20 , when the reference power changes from 1 to 2 KW the current injected by the inverter changes.

IV. CONCLUSION

This paper proposed the study and the control of photovoltaic-Battery storage grid connected system, the use of a three level DCI with his simplified space vector modulation as a grid interface gives a good results in term of THD and power quality, also, the aim was in this work to inject to the grid a fixed power whatever solar irradiance and temperature condition. The results obtained from this performance analysis confirm that the control strategy adopted achieves the specified performance objectives

TABLE IV
SYSTEM PARAMETERS VALUES

Photovoltaic array			
Pmax	150	W	Maximal power
Vop	34.5	V	Optimal voltage
Iop	4.35	A	Optimal current
Voc	43.5	V	open circuit voltage
Icc	4.75	A	Short circuit current
Ns	18	1	Number of series arrays
Np	10	1	Number of parallel arrays
DC Bus			
Udc	432	V	DC bus voltage
Filter			
Rt	3	Ω	Filter resistance
Lt	0,06	H	Filter inductance
Grid			
Vs	380	V	voltage
f	50	Hz	frequency
Battery bank			
C_{10}	118	Ah	Battery capacity at 10-hour discharge rate
C_v	8	V^{-1}	Voltage coefficient
C_T	0.05	K^{-1}	Temperature coefficient
I_{go}	0.035	A	Normalised gassing current
$Q_{max,c}$	120	Ah	Maximum charge capacity
$Q_{max,d}$	130	Ah	Maximum discharge capacity
R_{ic}	75	mΩ	Internal resistance when charging the battery
R_{id}	38	mΩ	Internal resistance when discharging the battery
E_{0d}	11.6	V	Limiting internal battery voltage for zero current and fully discharged

ISSN: 2356-5608

			battery after the initial transient
A_c	0.01	-	Parameter reflecting the initial linear variation of the internal battery voltage with increasing state-of-charge
C_c	0.012	-	Parameter reflecting increasing voltage when battery is progressively charged
D_c	130	-	Parameter reflecting sharp increase of voltage when battery is charged to a high SOC
EF_c	0.45	-	Exponential factor introduced to achieve a closer curve fit for voltage behaviour when progressively charged
E_{0d}	12.6	V	Fully charged internal battery voltage when discharging after the initial transient
A_d	-0.007	-	Parameter reflecting the initial linear variation of the internal battery voltage with decreasing state-of-charge
C_d	-0.3	-	Parameter reflecting decreasing voltage when battery is progressively discharged
D_d	165	-	Parameter reflecting sharp decrease of voltage when battery is discharged to a low SOC
EF_d	1.25	-	Exponential factor introduced to achieve a closer curve fit for voltage behaviour when progressively discharged
C_1	0.0006	h/A^2	Parameter to calculate maximum charge capacity
C_2	0.0543	h/A	Parameter to calculate maximum charge capacity
C_3	2.0279	h	Parameter to calculate maximum charge capacity
C_4	140.29	Ah	Parameter to calculate maximum charge capacity
D_1	-0.0006	h/A^2	Parameter to calculate maximum discharge capacity
D_2	0.0543	h/A	Parameter to calculate maximum discharge capacity
D_3	-2.0279	h	Parameter to calculate maximum discharge capacity
D_4	140.29	Ah	Parameter to calculate maximum discharge capacity
B_s	36	-	Number of series batteries of 12 V

REFERENCES

1. L. Hassaine, E. Olı´as, Simulation of grid-interface connecting photovoltaic power systems. Proceedings of the World Renewable Energy Congress IX Florence, Italy, 2006.
2. N. Hamrouni_, M. Jraidi, A. Che´ rif. New control strategy for 2-stage grid-connected photovoltaic power system. Renewable Energy 33 (2008) 2212–2221.
3. A. AL-Amoudi, L. Zhanc, Optimal control of a grid-connected PV system for maximum power point tracking and unity power factor. On power electronics and variable speed drives. Seventh International Conference on (Conf. Publ. No. 456), London, 1998, pp. 80–85.
4. Wu T -F, Nien H-S, Shen C-L, Chen T -M. A single-phase inverter system for PV power injection and active power filtering with nonlinear inductor consideration. Transactions on Industry Application 2005 Jul–Aug;41(4):1075–83.
5. Dali M, Belhadj J, Roboam X. Hybrid solar-wind system with battery storage operating in grid connected and standalone mode: control and energy management-experimental investigation. Energy 2010;35(6):2587-95.
6 . Pouresmaeil E, Montesinos-Miracle D, Gomis-Bellmunt O, Bergas-Jané J.A multi-objective control strategy for grid connection of DG (distributed generation) resources. Energy 2010;35(12):5022-30.
7. Anna Rita Di Fazio, Mario Russo. Photovoltaic generator modelling to improve numerical robustness of EMT simulation. Electric Power Systems Research 83 (2012) 136– 143
8. Benjamin Wichert. Control of Photovoltaic Diesel Hybrid Energy Systems. PHD thesis of the Curtin University of T echnology. 2000.
9. S. Armstrong, M. E. Glavin, and W. G. Hurley, .Comparison of battery charging algorithms for stand-alone photovoltaic systems. IEEE Power Elect. Specialists Conference, 2008, pp. 1469-1475.
10. Alberto Lega. Multilevel Converters: Dual Two-Level Inverter Scheme. Ph.D. thesis. University of Bologna March 2007.
11. J.S. Lai, F.Z. Peng, Multilevel converters : a new breed of power converters. IEEE Transactions on Industry Applications 32 (May (3)) (1996),pp. 509–517.
12. N. Celanovic. Space vector modulation and control of multilevel converters. PhD thesis, Virginia Polytechnic Institute and State University, Blacksburg, Virginia, USA, 2000.
13. Lalili D. Berkouk E. M., Boudjema F. , Lourci N.,Taleb T. and Petzold, J. Simplified space vector PWM algorithm for three-level inverter with neutral point potential control, The Medeteranean Journal of Measurement and Control. vol 3, No 1, (2007), pp.30-39.
14. F. Blaabjerg, R. Teodorescu, M. Liserre, and A. Timbus. Overview of Control and Grid Synchronization for Distributed Power Generation Systems. IEEE Trans. Ind. Electron., vol. 53, no. 5, pp. 1398-1409, Oct. 2006.
15. Bouchafaa F, Beriber D, Boucherit M.S. Modeling and control of a gird connected PV generation system. In: 18th Mediterranean Conference on Control & Automation, 2010. pp. 315–320.

ISSN: 2356-5608